Thermal metadevices with geometrically anisotropic heterogeneous composites

Boyan Tian[a], Jun Wang[a,*], Gaole Dai[b], Xiaoping Ouyang[c], Jiping Huang[a]

[a] Department of Physics, State Key Laboratory of Surface Physics, and Key Laboratory of Micro and Nano Photonic Structures (MOE), Fudan University, Shanghai 200433, China
[b] School of Sciences, Nantong University, Nantong 226019, China
[c] School of Materials Science and Engineering, Xiangtan University, Xiangtan 411105, China

ARTICLE INFO

ABSTRACT

The classical effective medium theory (EMT) provides a powerful tool in designing heterogeneous-composite functional thermal metadevices. But it is usually appropriate for spatially symmetric or geometrically isotropic systems, which limits the flexibility or adjustability in control. Here, we develop a generalized EMT to predict effective thermal conductivities of heterogeneous systems with elliptical (or ellipsoidal) inclusions. With the generalized EMT, omnidirectional thermal invisibility and directional Janus thermal illusion are designed and experimentally demonstrated just by tuning orientations of shape-anisotropy particles. In particular, we try to clarify the respective scopes of the generalized Maxwell-Garnett and Bruggeman theory based on both theoretical interpretations and numerical simulations. Our work may offer a promising fundamental framework and application prototype in elaborating thermal metadevices with asymmetry, irregularity, or anisotropy in configuration.

© 2021 Elsevier Ltd. All rights reserved.

1. Introduction

Designing thermal metamaterials usually depends on spatially-varying thermal parameters [1,2]. Various novel functions such as thermal cloaking [3–5], concentrating [5,6], transparency [7,8], or illusion [9,10] request specific thermal conductivity distribution in each functional zone. The requested thermal conductivities rarely exist in a single naturally-occurring material. So heterogeneous composites play core roles in realizing thermal metamaterials [11–15]. Then how to exactly predict effective thermal conductivities of composites becomes a significant topic in this field. With increasing complicated structures [16–19] and shrinking critical sizes [20,21] in thermal metadevices for elaborate control of heat flow, this issue will be extremely crucial.

Fortunately, the classical effective medium theory (EMT) provides a powerful framework for solving this problem [22,23]. Particularly, the Maxwell-Garnett (M-G) theory [24] and Bruggeman theory [25] often serve for handling multi-phase systems with asymmetry and symmetry in components, respectively. Generally, the EMT for treating such systems requests geometrical isotropy.

Saying, no shape factor of components is considered in the formulas. This category of system has been widely employed in thermal metamaterial design [26–28]. However, recent researches of thermal metamaterials have witnessed a growing focus on anisotropic [29–31], asymmetry [32–35] or irregular [36,37] configurations. Elliptical-particle composites [29,30,36,37] have shown potentials in realizing unprecedented functionalities beyond cycloidal-particle ones due to their high degrees of freedom in control. But the EMT for handling such geometrically-anisotropic thermal systems is unsatisfactory. The generalized EMT of geometrically anisotropic composite systems in electromagnetism [38–41] was built previously, but its counterparts in thermotics is still fragmentary and inadequate. This may be because of the intrinsic difference between electromagnetics and thermotics. Particularly, some concepts such as frequency or chromatic dispersion have no analogy in thermal diffusion systems. Another issue is that the applicative conditions of the M-G theory and Bruggeman theory in thermotics are not clearly identified. Although they may be approximately equivalent in predicting effective thermal conductivities of asymmetrical-component systems (for example, magnetic nanofluids [42,43]), it is essential to clarify the criteria of these two theories.

To solve the problems mentioned above, we systematically formulate the generalized EMT for geometrically-anisotropic hetero-

---

* Corresponding author.:
E-mail addresses: 18110190048@fudan.edu.cn (J. Wang), oyxp2003@aliyun.com (X. Ouyang), jphuang@fudan.edu.cn (J. Huang).
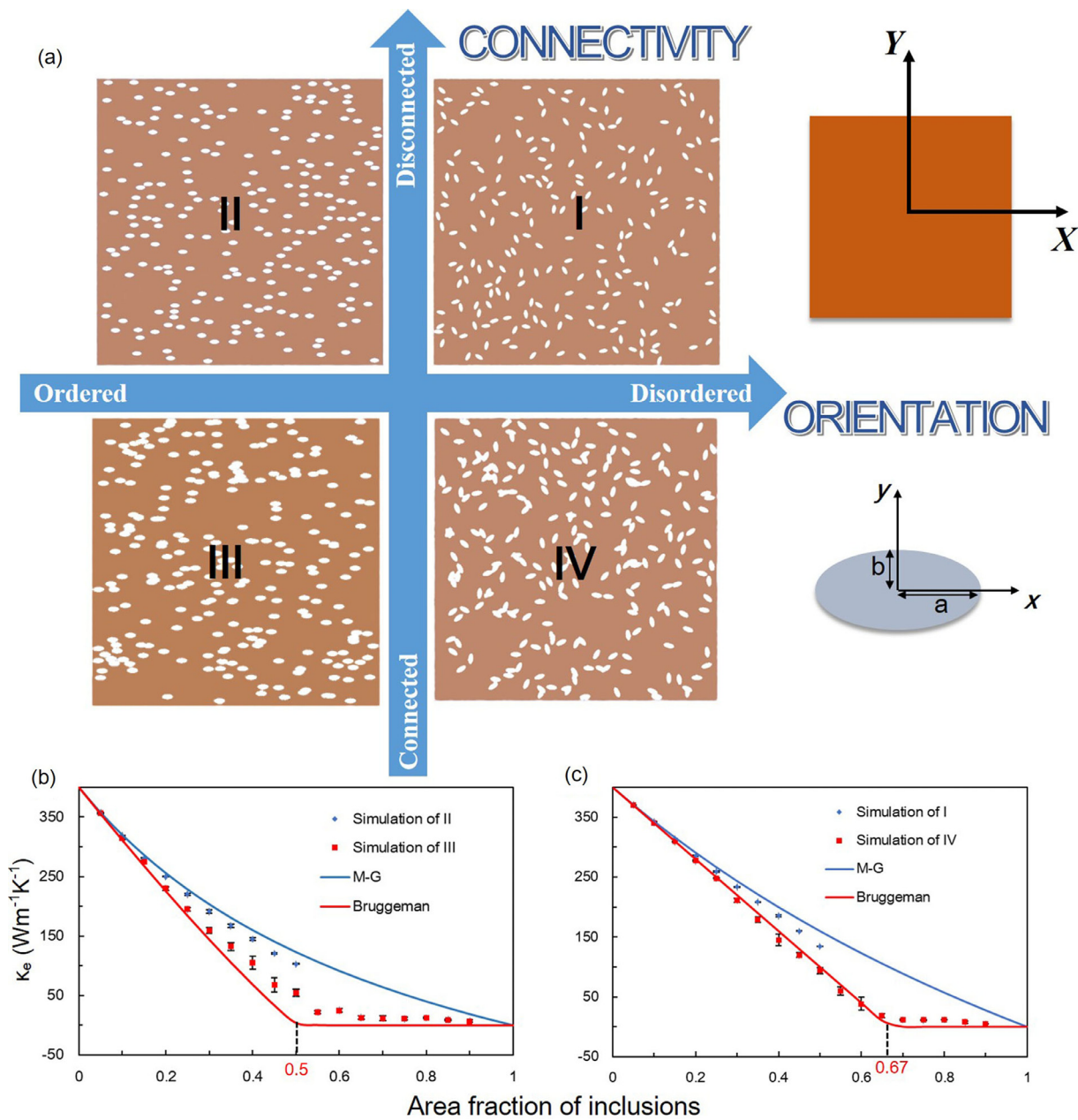
Fig. 1. (a) Heterogeneous composites are categorized in the four-quadrant system by particles' orientation and connection. Two sets of coordinates are built on the matrix and elliptical inclusion respectively, which denote to the main coordinate (X, Y) and sub-coordinate (x, y). (b)-(c) Theory and simulation results of the effective thermal conductivities on particle-area-fraction dependence, which are based on the four models in (a). I and II are corresponding to the generalized M-G (blue line) theory and III and IV are corresponding to the generalized Bruggeman (red line) theory. The thermal conductivities of matrix and inclusion are 400 and 0.026 $Wm^{-1}K^{-1}$, which can be regarded as $\kappa_m \gg \kappa_i$. The quantity and aspect ratio of inclusions are kept at 225 and 2 : 1. Error bars are marked in black, which denote standard deviation of three-times simulations at each simulated area-fraction position.

geneous thermal systems based on the mean-field-approximation concept. Without loss of generality, we start from the two-dimensional inclusion-matrix models, and classify heterogeneous composites by elliptical (or ellipsoidal) inclusions' orientation and connectivity; see Fig. 1. We discuss the concrete forms of generalized EMT by applying them to these four models shown in Fig. 1, and reveal the underlying mechanisms of corresponding theories. With the help of additional orientation control in such geometrically-anisotropic systems, omnidirectional thermal invisibility and directional Janus thermal illusion can be achieved just by adjusting main-axis directions of inclusions. Here, the former means no distortion in backgrounds regardless of heat sources' positions, while the latter denotes different illusions if boundary heat sources are applied at different directions.

2. Theory

First, we consider an infinite-matrix approximation model to ignore non-local effects for simplification of analyses. The elliptical particles are embedded in an isotropic matrix in random distribution without connection. Because percolation is inhibited in this system, the M-G theory is usually employed for treating this case. We set two groups of Cartesian coordinate systems to facilitate analyses. One is fixed on the matrix as the main coordinate (X, Y), and the other is fixed on each elliptical particle as the sub-coordinates (x, y), as the right panel of Fig. 1(a) shown. We can give the expression of effective thermal conductivity in (X, Y) as

$$\boldsymbol{\kappa}_e = \begin{bmatrix} \kappa_{eX} & \\ & \kappa_{eY} \end{bmatrix}. \tag{1}$$

Generally, in linear diffusive systems, flow has a linear relation with force. Supposing a thermal field (external temperature gradient) $\boldsymbol{E}_0$ is applied along the X axis, the effective thermal conductivity κ_{eX} of this system can be defined according to the mean-field theory:

$$\kappa_{eX} = \frac{\langle \boldsymbol{J}_{tot} \rangle}{\langle \boldsymbol{E}_{tot} \rangle} = \frac{f_i \langle \boldsymbol{J}_i \rangle + f_m \langle \boldsymbol{J}_m \rangle}{f_i \langle \boldsymbol{E}_i \rangle + f_m \langle \boldsymbol{E}_m \rangle} = \frac{f_i \kappa_i \langle \boldsymbol{E}_i \rangle + f_m \kappa_m \langle \boldsymbol{E}_m \rangle}{f_i \langle \boldsymbol{E}_i \rangle + f_m \langle \boldsymbol{E}_m \rangle}, \tag{2}$$

where the symbol $\langle ... \rangle$ means statistical average over the area. $\boldsymbol{J}$ and $\boldsymbol{E}$ are heat flow and thermal field respectively. Subscripts tot, i and m refer to total medium, inclusion and matrix. f and κ are the area fraction and thermal conductivity respectively. Eq. (2) implies that total heat flows and thermal fields are statistical averages of local flows and fields. We introduce the field factor η to describe the relation between the inclusion thermal field $\langle \boldsymbol{E}_i \rangle$ and the external thermal field $\langle \boldsymbol{E}_0 \rangle$ as

$$\langle \boldsymbol{E}_i \rangle = \eta \boldsymbol{E}_0. \tag{3}$$

And the matrix thermal field can be written as

$$\langle \boldsymbol{E}_m \rangle = \boldsymbol{E}_0, \tag{4}$$

due to the infinite matrix approximation [30]. Then, Eq. (2) becomes

$$\kappa_{eX} = \frac{f_i \eta \kappa_i + f_m \kappa_m}{f_i \eta + f_m}. \tag{5}$$

An explicit definition of orientation is that "ordered" means (x, y) overlaps with (X, Y), while "disordered" means (x, y) spins equiprobably in (X, Y). So for the orderly-oriented model (quadrant II in Fig. 1(a)), η is expressed as

$$\eta_{II} = \frac{\kappa_m}{\kappa_m + g_x(\kappa_i - \kappa_m)}. \tag{6}$$

And for the disorderly-oriented model (quadrant I in Fig. 1(a)), η is expressed as

$$\eta_I = \frac{1}{2}\left[\frac{\kappa_m}{\kappa_m + g_x(\kappa_i - \kappa_m)} + \frac{\kappa_m}{\kappa_m + g_y(\kappa_i - \kappa_m)} \right]. \tag{7}$$

g_x and g_x are depolarization factors of elliptical particles along main axes and secondary axes. Detailed descriptions of depolarization factors can be found in the Appendix A1. Substituting Eqs. (6) and (7) into Eq. (5) and combining with $f_i + f_m = 1$, we can obtain the generalized M-G theory as

$$\kappa_{eX} = \kappa_m + \frac{f_i \frac{\kappa_i - \kappa_m}{\kappa_m + g_x(\kappa_i - \kappa_m)}}{1 - f_i \frac{g_x(\kappa_i - \kappa_m)}{\kappa_m + g_x(\kappa_i - \kappa_m)}} \kappa_m, \tag{8a}$$

$$\kappa_{eY} = \kappa_m + \frac{f_i \frac{\kappa_i - \kappa_m}{\kappa_m + g_y(\kappa_i - \kappa_m)}}{1 - f_i \frac{g_y(\kappa_i - \kappa_m)}{\kappa_m + g_y(\kappa_i - \kappa_m)}} \kappa_m \tag{8b}$$

for ordered-orientation systems and

$$\kappa_{eX} = \kappa_{eY} = \kappa_m + \frac{f_i \left[\frac{\kappa_i - \kappa_m}{\kappa_m + g_x(\kappa_i - \kappa_m)} + \frac{\kappa_i - \kappa_m}{\kappa_m + g_y(\kappa_i - \kappa_m)} \right]}{2 - f_i \left[\frac{g_x(\kappa_i - \kappa_m)}{\kappa_m + g_x(\kappa_i - \kappa_m)} + \frac{g_y(\kappa_i - \kappa_m)}{\kappa_m + g_y(\kappa_i - \kappa_m)} \right]} \kappa_m \tag{9}$$

for disordered-orientation systems.

Till now, we have derived the generalized M-G theory in consideration of unconnected inclusions. However, if particles are allowed to interconnect (quadrant III and IV in Fig. 1(a)), percolation may occur even though the area fraction of particles is very small. This means matrix and inclusion play equivalent roles in determining the effective thermal conductivity of composite. So we have to resort to the Bruggeman theory for treating this case. Following Ref. [39], when particles' main axes orient along the X axis [quadrant III in Fig. 1(a)] or totally disorderly [quadrant IV in Fig. 1(a)],

the corresponding polarizability β of inclusions and matrixes corresponding to III and IV can be written as

$$\beta_{III} = \frac{\kappa_k - \kappa_{eX}}{\kappa_{eX} + g_x(\kappa_k - \kappa_{eX})} \tag{10}$$

and

$$\beta_{IV} = \frac{1}{2}\left[\frac{\kappa_k - \kappa_{eX}}{\kappa_{eX} + g_x(\kappa_k - \kappa_{eX})} + \frac{\kappa_k - \kappa_{eY}}{\kappa_{eY} + g_y(\kappa_k - \kappa_{eY})} \right], \tag{11}$$

where the subscript $k = i, m$ for inclusion and matrix respectively. Taking the self-consistent condition $\sum_k f_k \beta_k = 0$, which means elimination of components' impact on the effective medium, we can write the generalized Bruggeman theory of binary inclusion-matrix systems as

$$f_i \frac{\kappa_i - \kappa_{eX}}{\kappa_{eX} + g_x(\kappa_i - \kappa_{eX})} + (1 - f_i) \frac{\kappa_m - \kappa_{eX}}{\kappa_{eX} + g_x(\kappa_m - \kappa_{eX})} = 0, \tag{12a}$$

$$f_i \frac{\kappa_i - \kappa_{eY}}{\kappa_{eY} + g_y(\kappa_i - \kappa_{eY})} + (1 - f_i) \frac{\kappa_m - \kappa_{eY}}{\kappa_{eY} + g_y(\kappa_m - \kappa_{eY})} = 0 \tag{12b}$$

for ordered-orientation systems and

$$f_i \left[\frac{\kappa_i - \kappa_{eX}}{\kappa_{eX} + g_x(\kappa_i - \kappa_{eX})} + \frac{\kappa_i - \kappa_{eX}}{\kappa_{eX} + g_y(\kappa_i - \kappa_{eX})} \right] + (1 - f_i) \left[\frac{\kappa_m - \kappa_{eX}}{\kappa_{eX} + g_x(\kappa_m - \kappa_{eX})} + \frac{\kappa_m - \kappa_{eX}}{\kappa_{eX} + g_y(\kappa_m - \kappa_{eX})} \right] = 0 \tag{13}$$

for disordered-orientation systems. It is noted that κ_{eX} can also be replaced by κ_{eY} in Eq. (13) due to isotropic effective thermal conductivities in this case.

Hereto, we have obtained the generalized M-G theory and Bruggeman theory for calculating two-dimensional and two-component elliptical-particle-embedded composites' thermal conductivities. We can readily expand these results to d-dimensional and n-component systems. Then there will be $n - 1$ kinds of inclusions with different f_i and κ_i and one matrix. And each kind of inclusion has d dimensions. We still consider the X-axis directions. The common form of generalized M-G theory can be expressed as

$$\kappa_{eX} = \kappa_m + \frac{\sum_{i=1}^{n-1} f_i \frac{\kappa_i - \kappa_m}{\kappa_m + g_{ix}(\kappa_i - \kappa_m)}}{1 - \sum_{i=1}^{n-1} f_i \frac{g_{ix}(\kappa_i - \kappa_m)}{\kappa_m + g_{ix}(\kappa_i - \kappa_m)}} \kappa_m \tag{14}$$

for ordered-orientation systems and

$$\kappa_{eX} = \kappa_{eY} = \kappa_m + \frac{\sum_{i=1}^{n-1} f_i \sum_{j=1}^{d} \frac{\kappa_i - \kappa_m}{\kappa_m + g_{ij}(\kappa_i - \kappa_m)}}{d - \sum_{i=1}^{n-1} f_i \sum_{j=1}^{d} \frac{g_{ij}(\kappa_i - \kappa_m)}{\kappa_m + g_{ij}(\kappa_i - \kappa_m)}} \kappa_m \tag{15}$$

for disordered-orientation systems. Similarly, with self-consistent condition $\sum_i f_i \beta_i = 0$, the generic form of generalized Bruggeman theory can be written as

$$\sum_{i=1}^{n} f_i \frac{\kappa_i - \kappa_{eX}}{\kappa_{e\_B1} + g_{ix}(\kappa_i - \kappa_{eX})} = 0 \tag{16}$$

for ordered-orientation systems and

$$\sum_{i=1}^{n} f_i \sum_{j=1}^{d} \frac{\kappa_i - \kappa_{eX}}{\kappa_{eX} + g_{ij}(\kappa_i - \kappa_{eX})} = 0 \tag{17}$$
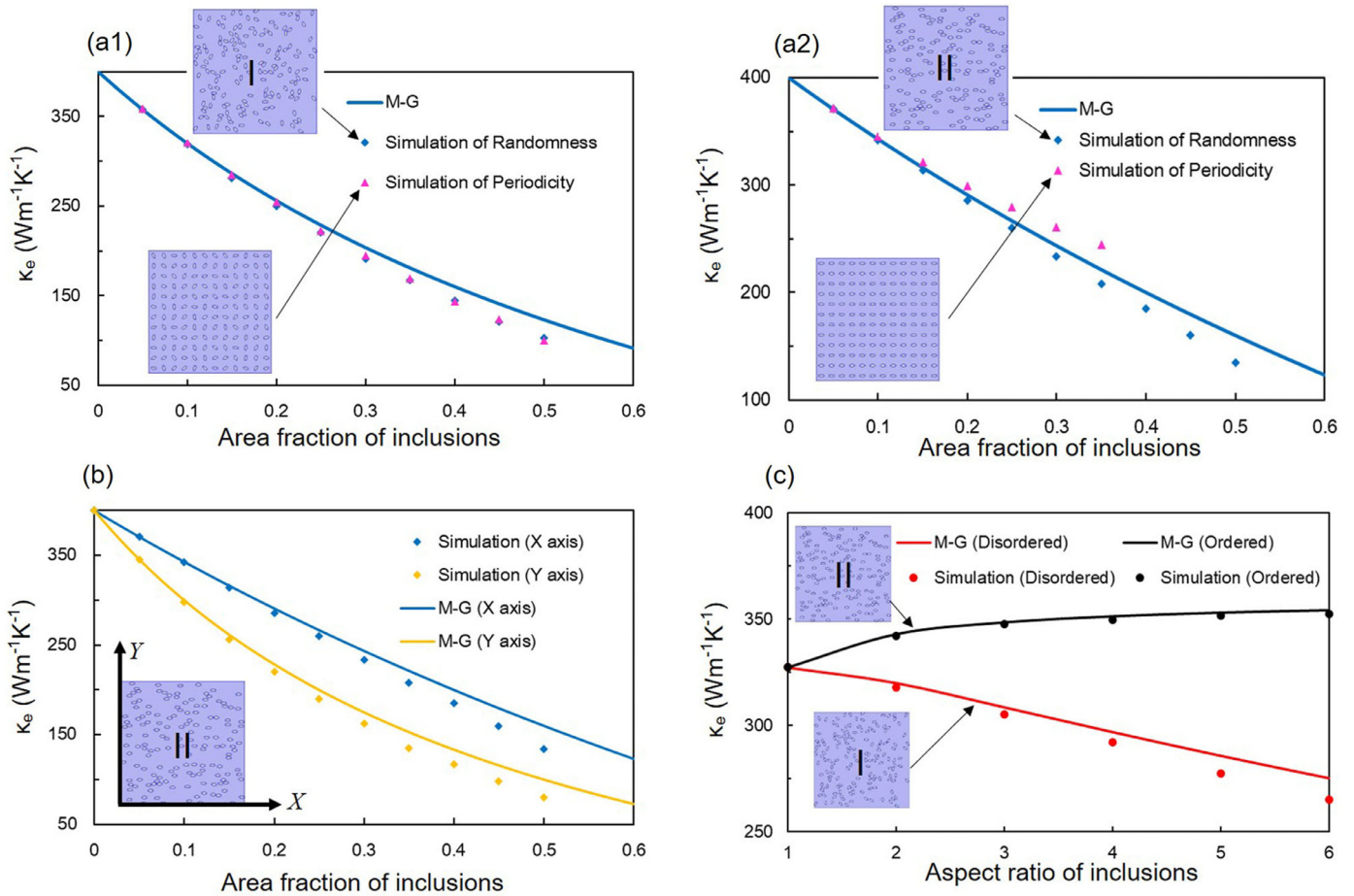
for disordered-orientation systems.

Fig. 2. Theoretical predictions and finite-element simulations of the generalized M-G theory [corresponding to model I and II in Fig. 1 (a)] for checking effects of periodicity [(a1) and (a2)], direction (b), and aspect ratio (c). The thermal conductivities of matrix and inclusion are 400 and 0.026 Wm^{-1}K^{-1}. (a1) and (a2) Theoretical predictions and simulation results of effective thermal conductivities on area-fraction dependence. Specifically, we show the simulations of periodic-distribution models (pink dots) for comparison. In (a2), main axes of elliptical particles orient along the X axis. (b) Theoretical and corresponding simulation results of effective thermal conductivities in X (blue line or dots) and Y (yellow line or dots) directions. The model is model II. (c) Aspect-ratio-dependent relations of effective thermal conductivities. Here we only check the X direction's values. Red and black lines and dots denote disordered (I) and ordered (II) systems respectively.

3. Numerical analyses and simulations

Here, we are in the position to verify the deduced generalized M-G and Bruggeman theory [Eqs. (8)-(9) and (12)-(13)] by finite-element simulations. The common commercial software COMSOL Multiphysics [44] is employed for executing simulations. We adopt the models shown in Fig. 1(a) and compare their simulation results with the theoretical predictions. These quantitative verifications of two-component case can be trivially expanded to the n-component one. Particularly, the thermal conductivities of particles and matrixes are set as 0.026 and 400 Wm^{-1}K^{-1} (which approach air and copper respectively). Numbers of particles dispersing in the medium are taken as 225. We keep their aspect ratios to be 2 : 1 as a typical case of geometrically-anisotropic inclusions. So the g_x and g_y can be calculated as $1/3$ and $2/3$ respectively. It is noted that the upper-bound area fractions of case I and II are 0.5, which is an automatical truncation point in our computing procedures. This is because particles are not allowed to connect each other, which can be interpreted by the close packing theory of axisymmetric particles [45]. On the other hand, case III and IV do not have this limition. E_0 is applied along the X axis. Comparing Eqs. (8)-(9) and Eqs. (12)-(13) [corresponding to the blue and red solid lines in Figs. 1(b) and (c)], we can see diametrically different effective-thermal-conductivity predictions. The theoretical percolation threshold of red lines can be analytically obtained by taking $\kappa_i = 0$ in Eqs. (12)-(13). In detail, for example, the perco-

lation threshold of area fraction in Eq. (12) is calculated to be $f_c = 1 - g_x = 1 - 1/3 = 2/3$, and the effective thermal conductivity can thus be expressed as

$$\kappa_{eX} = \begin{cases} \kappa_m \times (1 - f_i/f_c), & f_i < 2/3 \\ 0. & f_i \geq 2/3 \end{cases} \tag{18}$$

We execute simulations in each area point for five times and take their averages and standard deviations, which are shown as simulation points and error bars in Figs. 1(b) and (c). The simulation results echo with the according theories, verifying our assumption that the generalized M-G and Bruggeman theories can be classified by whether there existing interconnection between inclusions.

We further check the effects of periodicity, direction, and aspect ratio on generalized M-G theory, see Fig. 2. This will facilitate device design. Figs. 2(a1) and (a2) show comparisons of the generalized M-G theory and simulation results of random or periodic composites. Periodicity is formed by a 15×15 particle array. The quantity of particles keep equal to the random case in our simulations. We can see the simulation results almost fit the M-G theory. But stronger inclusive interaction in periodic systems may introduce more impacts on the accuracy of theoretical predictions, which will deviate from the M-G theory. Besides, we check the direction effects of particles described in Eq. (8), see Fig. 2(b). There is no obvious major- or minor- axis effects on the prediction accuracy. Saying, whether major or minor axes
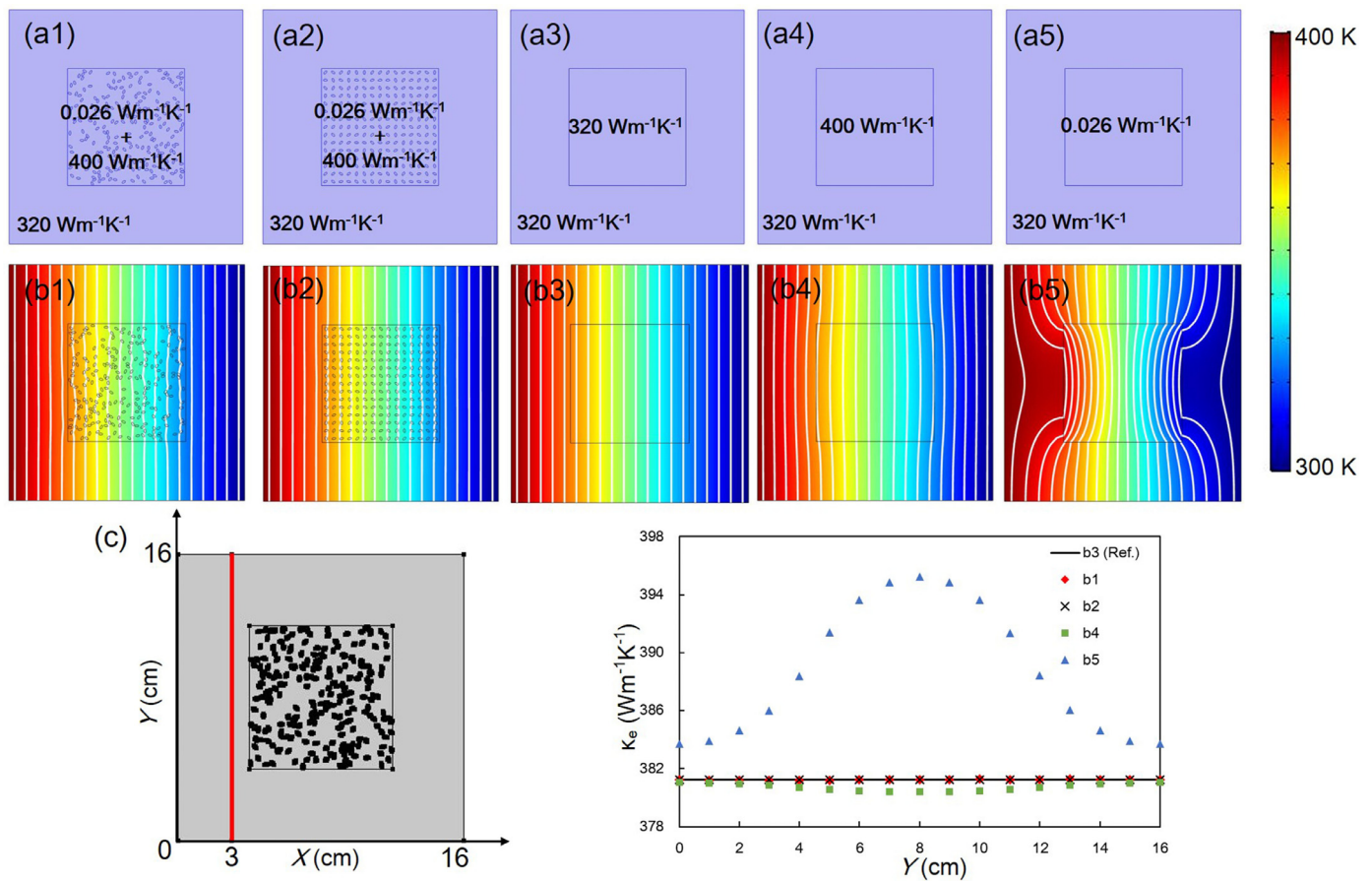
Fig. 3. Simulations of omnidirectional thermal invisibility under line-heat-source conditions. Heat (400 K) and cold (300 K) sources are applied on left and right boundaries of devices. Backgrounds and central composites are 16 × 16 cm and 8 × 8 cm in size. Composites are matrix plus disorderly-oriented inclusions with random (a1) or periodic (a2) distributions. Another three reference groups are constructed by replacing central composites with sole background materials (a3), matrix materials (a4), and inclusion materials (a5). (b1)-(b5) are corresponding temperature distributions of (a1)-(a5) with isothermal lines in white. (c) Left panel is a sketch model for showing the data-extraction position marked in a red line. Right panel is the extracted data from (b1)-(b5) at red-line positions.

are along $\boldsymbol{E}_0$, the derived theories have similar performances on effective-thermal-conductivity predictions. Furthermore, we study the aspect-ratio effects, see Fig. 2(c). The area fraction f_i is kept at 0.1. Aspect ratio $(a : b)$ varies from 1 : 1 (circle) to 6 : 1 (nearly rod-like). Effective thermal conductivities are changing with aspect ratios, which is verified by both theory and simulation. Particularly, ordered (black line and dots) and disordered (red line and dots) orientations of particles lead to deviating trend of effective thermal conductivities with increasing aspect ratios. This is a specific phenomenon which is inexistent in the classical M-G theory. The aspect-ratio effects on κ_e may contribute to designing continuously adjustable thermal conductivities with fixed-proportion composites.

4. Device design and experimental verification

Disordered and ordered orientations of particles lead to isotropy and anisotropy in effective thermal conductivities. This feature will help design multiple thermal metadevices just by adjusting particles' orientations. Here, we demonstrate omnidirectional thermal invisibility and Janus thermal illusion based on the generalized EMT. Although these two functionalities have been realized in thermal systems, we refresh them by employing geometrical anisotropy in inclusions of composites. We first propose omnidirectional thermal invisibility with disorderly-oriented inclusions plus isotropic matrix, see Fig. 3. Invisibility is defined as no distortion of isothermal lines through the whole device. The thermal conductivities of inclusions and matrix are 0.026 and 400 Wm^{-1}K^{-1} respectively. Congruent ellipses with 2 : 1 in aspect ratios are adopted as inclusions, whose total area fraction is kept at 0.1, which can be appropriately predicted by the generalized M-G theory [see Fig. 1(c)]. With these conditions, the effective thermal conductivity is calculated to be 320 Wm^{-1}K^{-1} by Eq. (9). This value is fixed as the background in our design. We adopt two sorts of particle distributions as randomness [Fig. 3(a1)]and periodicity [Fig. 3(a2)], and all inclusions are restricted in a 8 × 8 cm sub-domain. The sub-domain is located in the center of the square background whose size $(L \times L)$ is 16 × 16 cm. The right three reference groups are sole background material [Fig. 3(a3)], sole matrix material [Fig. 3(a4)], and sole inclusion material [Fig. 3(a5)] embedded in the background. A 400 K heat source and a 300 K cold source are placed at left and right boundaries respectively, and upper and lower boundaries are kept thermally isolated, Figs. 3(b1) and (b2) show in-plane thermal invisibility, nearly equivalent to Fig. 3(b3). Some small shift of isothermal line at interfaces is due to the limited quantity of particles. As a contrast, Figs. 3(b4) and (b5) show obvious temperature deviations from Fig. 3(b3). This is caused by thermal-conductivity mismatch between composites and backgrounds. We can check temperature data on a vertical line as shown in Fig. 3(c) for quantitative comparison. The red-marked line is located at $x = 3$ cm. The temperature data of designed schemes in Figs. 3(b1) and (b2) accord well with Fig. 3(b3). For further verifying the omnidirectional feature of the designed invisibility, we replace line sources with point heat sources in Fig. 4.
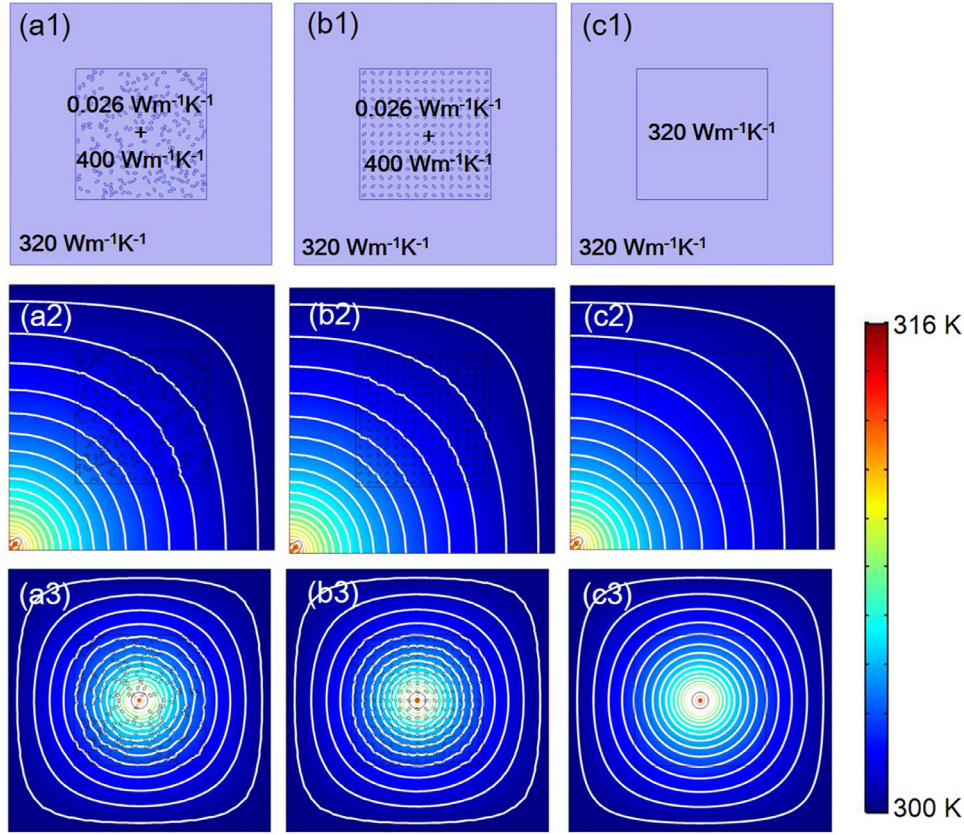
Fig. 4. Simulations of omnidirectional thermal invisibility under point-heat-source conditions. (a1)-(c1) are same as Figs. 3(a1)-(a3). (a2)-(c3) are corresponding temperature-distribution behaviors to (a1)-(c1). The point heat source is 0.5 cm in radius and 100 Wm^{-2} in power. In (a2)-(c2), we put it at the bottom-left positions and keep left and bottom boundaries heat-insulated. Top and right boundaries are kept at 300 K. In (a3)-(c3), we put it at the central positions and keep all boundaries at 300 K.

We take the same models as Figs. 3(a1)-(c1) in Figs. 4(a1)-(c1), and put the point sources at the bottom-left [Figs. 4(a2)-(c2)] and center [Figs. 4(a3)-(c3)]. The point source is kept at 0.5 cm radius in size and 100 Wm^{-2} in power. We can see similar isothermal line distributions in this three models, which confirms omnidirection of our invisibility design. The results also confirm the robustness of our design.

On the other hand, anisotropy in ordered-orientation systems can result in another illusion design, which is called Janus thermal illusion. Here, Janus refers to that devices show different functionalities or properties in different directions [13,46]. We still utilize the same area fractions and aspect ratios as Fig. 3, and just adjust the main-axis orientations of particles to be along the X axis, see Fig. 5. The effective thermal conductivities is then 343 and 300 Wm^{-1}K^{-1} in X and Y directions, respectively. Figs. 5(a1)-(c1) show three models containing a random system, a periodic system, and a reference. Figs. 5(a2)-(c3) show thermal invisibility along the horizontal axis and thermal illusion along the vertical axis, which form so-called Janus thermal illusion. We can see almost indistinguishable temperature distributions in backgrounds under X-axis E_0 [Figs. 5(a2)-(c2)]. Inversely. thermal illusion in Y-axis directions has distinct thermal distortions. The temperature feature can be mimicked by a uniform anisotropic material [Fig. 5(c1)] which has same thermal conductivities with the ordered-orientation systems in two different directions. The Janus illusion was demonstrated in periodic systems in Ref. [13]. Here we realize it with both random and periodic systems. This transferring is based on our theoretical and simulation results that the generalized M-G theory can predict the effective thermal conductivities both in random and periodic systems, especially at small inclusive area fractions.

Guided by the above design, experimental demonstrations are also performed. We employ copper slab whose thickness d is 0.3 cm and thermal conductivity is 400 Wm^{-1}K^{-1}. Holes are etched by laser ablation for realizing different thermal conductivity design in specific regions. The etched portion is regarded as air whose thermal conductivity is 0.026 Wm^{-1}K^{-1}. For obtaining uniform specific backgrounds, we etch periodic circular hole arrays and control their sizes by classical EMT [22], as shown in Figs. 6(a1)-(a5) and Figs. 7(a1) and (a2), respectively. Under the condition that heat and cold sources are placed at both sides, the heat channel may have three modes simultaneously through the plane, which are dominated by thermal conduction, convection, and radiation respectively. Our purpose is focusing on in-plane thermal conduction and eliminating the impact of other two out-of-plane factors. These three modes can be evaluated quantitatively by

$$J_{cond} = \kappa_e[(T_h - T_c)/L] * d * L, \tag{19a}$$

$$J_{conv} = h[(T_h + T_c)/2 - T_{amb}] * L^2, \tag{19b}$$

$$J_{rad} = \epsilon\sigma[((T_h + T_c)/2)^4 - T_{amb}^4] * L^2, \tag{19c}$$

where J_{cond}, J_{conv}, and J_{rad} refer to heat flow of conduction, convection, and radiation respectively. And κ_e, h, and ϵ denote to thermal conductivity, convective coefficient, and emissivity. As we keep $(T_h + T_c)/2$ approach to T_{amb}, J_{cond} is at least one order of magnitude larger than J_{conv} and J_{rad}. We cover the sample with a plastic film to block the natural convection through air holes and reduce the surface thermal radiation. And we place a foam board under the sample for the same purpose, and insulating direct impact of heat/cold sources as well. The omnidirectional thermal in-
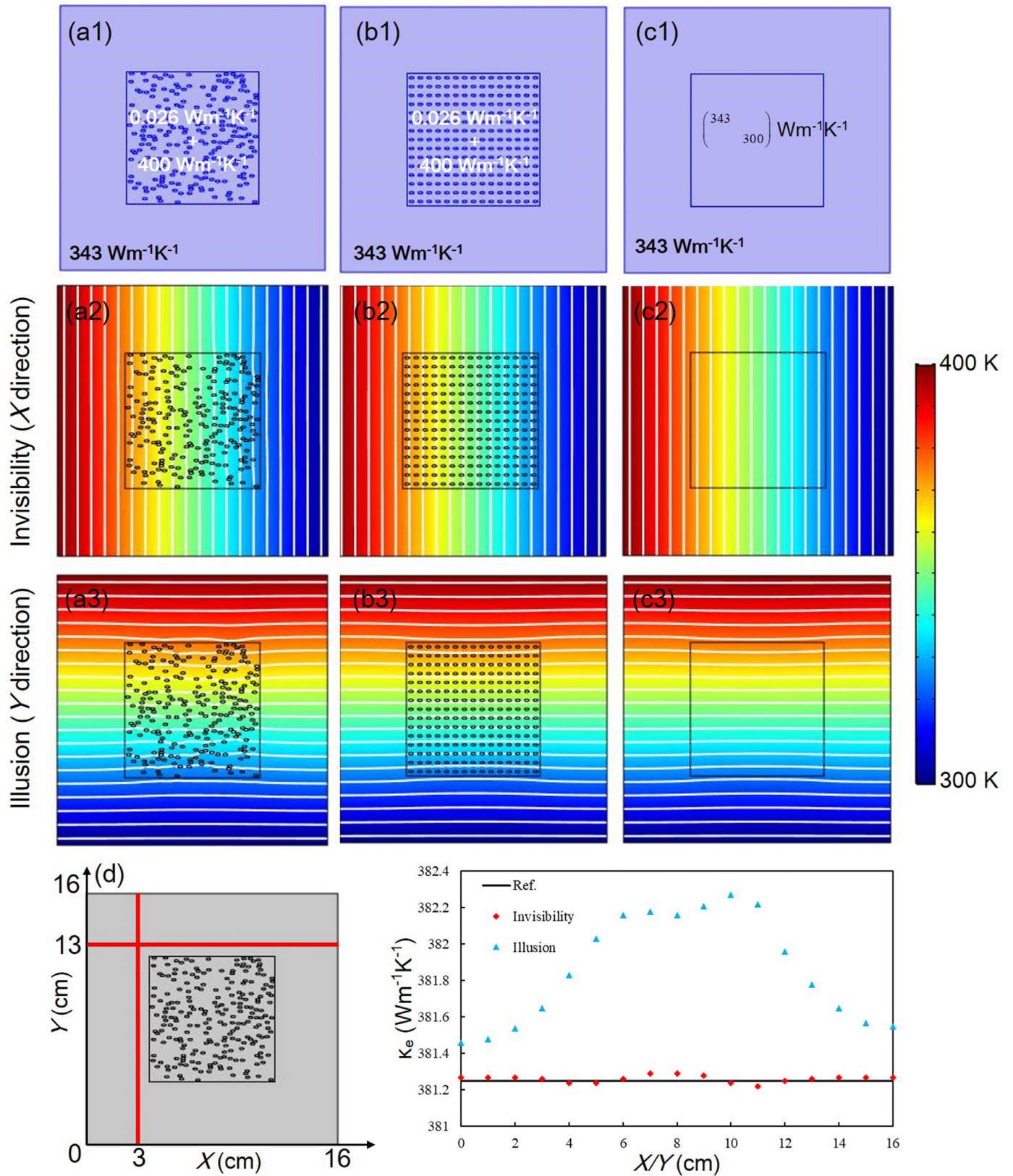
Fig. 5. Simulations of Janus thermal illusion. (a1)-(c1) are three models of random-distribution composite, random-distribution composite, and uniform anisotropic materials in the center. Sizes of them are same as Fig. 3. The composites are matrix plus orderly-oriented inclusions whose thermal conductivities are 400 and 0.026 Wm^{-1}K^{-1} respectively. Background's thermal conductivities are kept at 343 Wm^{-1}K^{-1}. Devices show thermal invisibility in X direction [(a2)-(c2)] and illusion in Y direction [(a3)-(c3)]. The extracted data at red line positions are from (a2) and (a3) respectively, shown in (d). The reference data in (d) is extracted from (c2) at $X = 3$ cm position.
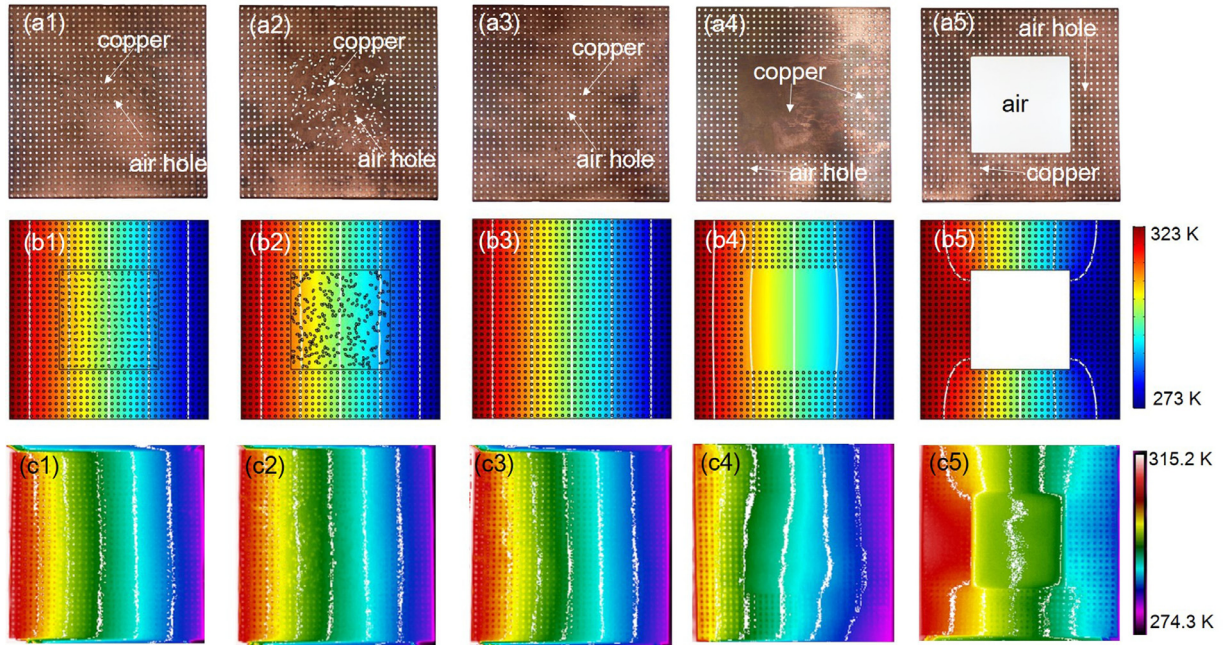
Fig. 6. Experimental design and results of thermal invisibility. (a1)-(a5) are five experimental samples, corresponding to Figs. 3(a1)-(a5). (b1)-(b5) are simulation results based on the structures in (a1)-(a5). (c1)-(c5) are actual experimental results based on (a1)-(a5) under the infrared camera. For matching their effective thermal conductivities, the background (400 $Wm^{-1}K^{-1}$) is etched and forming air hole (nearly 0.026 $Wm^{-1}K^{-1}$) array.
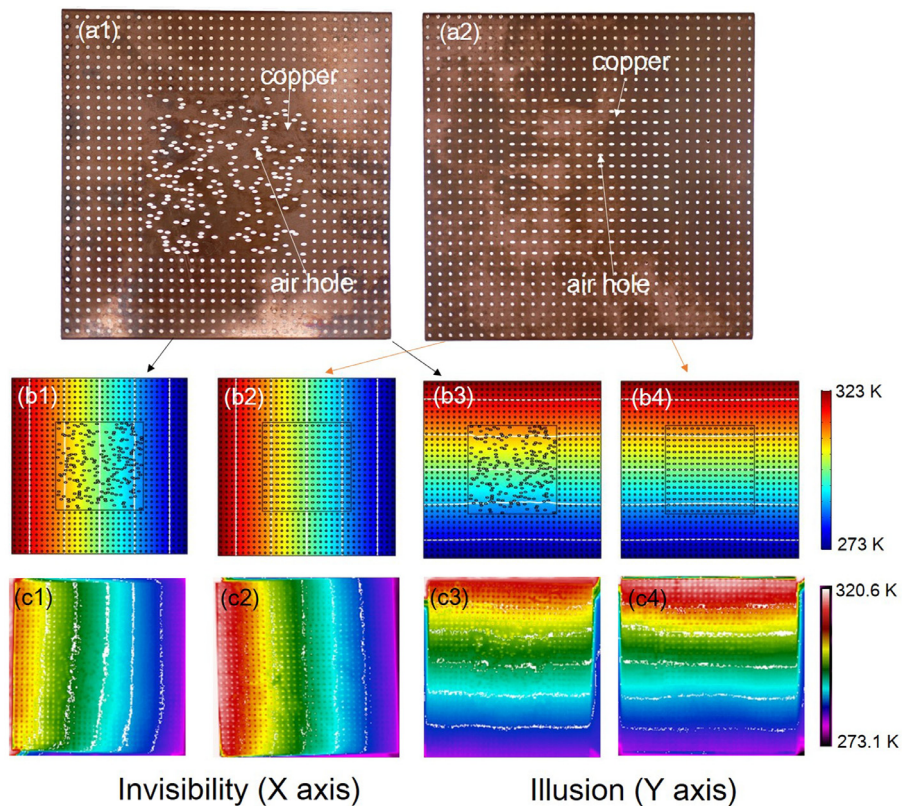

Fig. 7. Experimental design and results of Janus thermal illusion. (a1)-(a2) are two samples of random and periodic systems, corresponding to Figs. 5(a1) and (a2). (b1)-(b4) are simulation results based on the structures in (a1) and (a5). (c1)-(c4) are actual experimental results under the infrared camera. Temperature boundary conditions are applied along the X axis [(b1)-(b2)] or Y axis [(b3)-(b4)] respectively. For matching the effective thermal conductivities in (a1), the background (400 $Wm^{-1}K^{-1}$) is etched and forming air hole (nearly 0.026 $Wm^{-1}K^{-1}$) array.

visibility and directional Janus thermal illusion devices are thus manufactured, which accord with the parameters in the previous simulations. We also show the simulation results of these experimental samples which have elaborate patterns by COMSOL Mutilphyscis [44], see Figs. 6(b1)-(b5) and Figs. 7(b1)-(b4). By comparing the simulation and experimental temperature distributions in Figs. 6(c1)-(c5) and Figs. 7(c1)-(c4), the proposed thermal invisibility and Janus illusion is verified to be valid. It is noted that some distortions in white isotherms is because of the random fluctuation in random systems. Another probable factors is the random orientation deviates from the equal probability distribution. Increasing quantity of particles will eliminate these errors.

5. Discussion and conclusion

So far, we have discussed the generalized EMT with analytical theories and robust simulations. The results are readily expanded to d-dimensional and n-component systems. For further validating this statement, we design a three-component thermal invisibility metadevice in a three-dimensional system, Details can be seen in the Appendix A2. Starting from the Fourier's law, we give a macro-scale framework for calculating effective thermal conductivities of geometrically anisotropic heterogeneous composites. We should point out that infinite-matrix approximation is employed for eliminating non-local effects, which require the sizes of matrix are much larger than particles. Furthermore, while sizes of systems are decreased to micron or even nano scale, wave and particle effects of phonons will dominate in heat transport [48], and thus the generalized EMT becomes invalid. It is also noted that interface thermal resistance (ITR) [49] is not considered in theory and simulation. However, lattice mismatch or poor mechanical contact between different materials usually leads to the ITR issue. On the macro scale, the former is usually negligible. While the latter can be eliminated by filling the air voids at interfaces with soft matters (for example, polydimethylsiloxane) in experiments [5]. In terms of our experiment, we adopt air as the low-conductivity material by etching holes on copper films. So ITR caused by air gaps at interfaces is non-existent. Generally, ITR between two highly-different materials in thermal conductivities can be ignored, while it should be taken into account between two approximate-thermal-conductivity materials. Our experimental demonstrations on thermal invisibility and Janus thermal illusion provide a convinced demonstration in utilizing generalization of the conventional EMT, in which multiple functionalities are achieved by adjusting inclusion orientations. A common sense is that the Bruggeman theory is suitable for symmetrical systems, while the M-G theory applies to asymmetrical systems. This can be verified by invariance or variance after exchanging the subscripts in their respective formulas. Here, we try to provide a different viewpoint that interconnection between inclusions can induce symmetry between inclusions and matrix, which is suitable for the Bruggeman theory. Even if the great difference in proportion between matrix and inclusions, this result is still valid. We suggest that interconnection case can be interpreted by the percolation model, which is implied in the Bruggeman theory. Saying, although fillings of inclusions are small, interconnection between inclusions will still have probability to form global connections, just like that of the matrix. On the contrary, large filling fractions (even equivalent to the matrix) with non-connected particles never lead to percolation, and thus should be treated by the M-G theory.

Besides, there are three points to be noted: (1) The generalized M-G theory predicts better in random-distribution systems than in periodic-distribution systems. This is because of the more prominent interaction between periodically-distributed inclusions, which is not considered in the M-G formulations. Under the dilute limit, this interaction in both systems is negligible. Essentially, the M-G

theory is a discrete dipole approximation [47]. For more exact prediction in periodic-distribution systems, one correctional method is employing the Rayleigh approach [50,51] for introducing the interaction terms into the formulas, which is also called the multipole method. (2) The depolarization factor of elliptical inclusion is incompletely equivalent to the shape factor if the thermal conductivity is anisotropic. So in disordered cases, the anisotropy of effective thermal conductivity may be taken into consideration [43]. But we show in Appendix A1 that the difference between them is minor enough to be neglected in many actual experimental situations. (3) Another common sense is that effective thermal conductivities can be regulated by adjusting the fraction of inclusions in heterogeneous composites. However, with anisotropy in inclusions' shape, effective thermal conductivities are changing with aspect ratios, even if the filling fractions are fixed. This feature provides another degree of freedom for realizing specific thermal conductivities in thermal metamaterial design. Furthermore, continuous transformation on thermal conductivities can be achieved with the anisotropic morphology's gradual variation. While this is usually realized by filling fractions' variation on composites or phase change process on phase-changing materials.

In conclusion, we report thermal metadevices to realize omnidirectional invisibility and directional Janus illusion by tuning the elliptical inclusions' orientation. The generalized effective medium theory is developed for treating this kind of geometrically anisotropic heterogeneous composite. These results are valid even under extreme conditions and arbitrary shapes, so long as the linear steady-state heat transport is satisfied in the system. The presented theory and applications may provide solid fundamentals in highly freedom-of-control thermal metamaterial design with shape-anisotropy composites.

Declaration of Competing Interest

The authors declare that there are no conflicts of interest.

CRediT authorship contribution statement

Boyan Tian: Formal analysis, Writing - original draft. **Jun Wang:** Conceptualization, Formal analysis, Writing - original draft. **Gaole Dai:** Formal analysis, Writing - original draft. **Xiaoping Ouyang:** Formal analysis. **Jiping Huang:** Conceptualization, Formal analysis, Writing - original draft.

Acknowledgments

Appendix. A1. Depolarization factors

The depolarization factor can be approximatively regarded as the shape factor, which is only shape-related. For two-dimensional cases, we set the lengths of major and minor axis of ellipses to be a and b respectively. So g_x and g_y are written as

$$g_x = \frac{ab}{2} \int_0^\infty \frac{ds}{(a^2+s)\sqrt{(a^2+s)(b^2+s)}},$$
$$g_y = \frac{ab}{2} \int_0^\infty \frac{ds}{(b^2+s)\sqrt{(a^2+s)(b^2+s)}}. \tag{A1}$$

It is noted that $g_x + g_y = 1$. But for a more accurate description, it should consider anisotropy in the effective thermal conductivities. For the order-orientation case, effective thermal conductivities should be anisotropic. Anisotropy will make depolarization factors
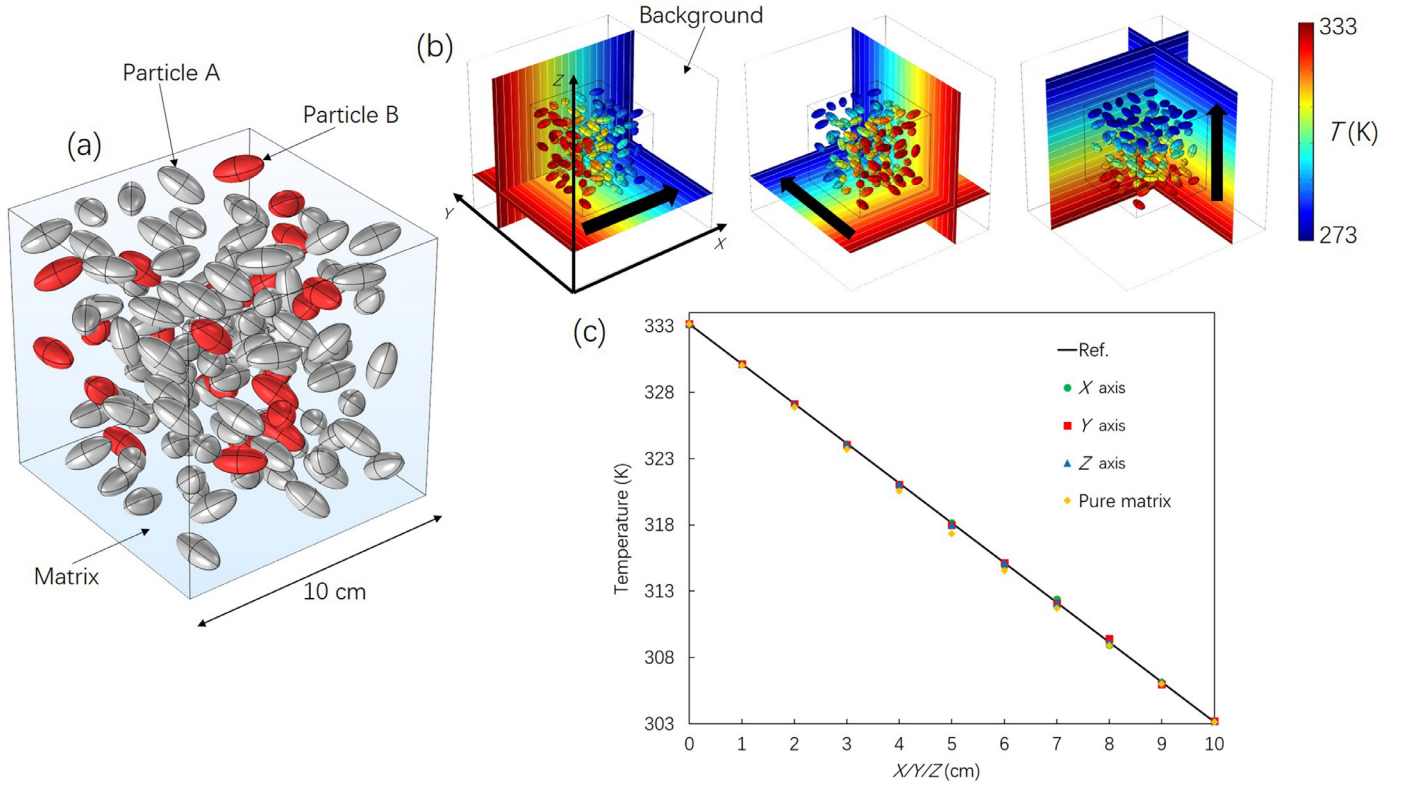
Fig. A1. Design and numerical simulations of three-dimensional three-component thermal invisibility. (a) Model design. Two sorts of ellipsoid particles (distinguished by different colors) share same sizes, 125 ellipsoid particles are divided into two categories (distinguished by different colors) with identical sizes, among which there are 100 gray and 25 red particles. Their intrinsic thermal conductivities are 1 and 100 for gray and red particles, respectively. The total volume proportion is 0.1. (b) Numerical simulations under 273–333 K temperature boundary conditions along X, Y, and Z axes. (c) Curve graph of temperature data versus position. The line is the pure background case by calculation and dots are extracted values of cubic center lines by simulation.

not accurately equivalent to shape factors [43]. So we need to use modified depolarization factors by considering anisotropy in effective thermal conductivities. Suppose that the x axis is parallel to the X axis, depolarization factors g_x and g_y should be modified as

$$g'_x = \frac{ab\kappa_{eX}}{2} \int_0^\infty \frac{ds}{(a^2+s\kappa_{eX})\sqrt{(a^2+s\kappa_{eX})(b^2+s\kappa_{eY})}},$$
$$g'_y = \frac{ab\kappa_{eY}}{2} \int_0^\infty \frac{ds}{(b^2+s\kappa_{eY})\sqrt{(a^2+s\kappa_{eX})(b^2+s\kappa_{eY})}}. \quad (A2)$$

We re-calculate the M-G plot with the correctional Eqs. (A2). It is less than 4% between original and revised predictions at the maximum deviation position. Considering the complexity of Eqs. (A2), it is reasonable to simplify it with the shape factor directly in most cases.

For three-dimensional cases, we suppose that l_j is the semi-axis length of direction j. Depolarization factors can be calculated as

$$g_j = \frac{abc}{2} \int_0^\infty \frac{ds}{(l_j^2+s)\sqrt{(a^2+s)(b^2+s)(c^2+s)}} \quad (A3)$$

where a, b, and c are three components of semi-axis lengths and $l_j = a, b,$ or c.

Appendix. A2. Design of three-dimensional three-component thermal invisibility metadevice

Here, we demonstrate a composite of two sorts of ellipsoid particles embedded in a cubic matrix with random orientation, which is a three-dimensional analogy to the designed two-dimensional thermal invisibility metadevice. The schematic diagram are shown

in Fig. A1(a). The ellipsoid particles are rotational ellipsoids with uniform a and b as major- and minor-axis lengths severally, and g_a and g_b are their respective depolarization factors. We set κ_1 and κ_2 as two intrinsic thermal conductivities of particles and κ_m as the thermal conductivity of background. Following Eq. (15), we can write down the effective thermal conductivity formula of this model as

$$\kappa_{e\_3D} = \kappa_m + \frac{\alpha + 2\beta + \gamma + 2\delta}{3 - (g_a\alpha + 2g_b\beta + g_a\gamma + 2g_b\delta)}\kappa_m \quad (A4)$$

where

$$\begin{cases} \alpha = \frac{\kappa_1-\kappa_m}{\kappa_m+g_a(\kappa_1-\kappa_m)} \\ \beta = \frac{\kappa_1-\kappa_m}{\kappa_m+g_b(\kappa_1-\kappa_m)} \\ \gamma = \frac{\kappa_2-\kappa_m}{\kappa_m+g_a(\kappa_2-\kappa_m)} \\ \delta = \frac{\kappa_2-\kappa_m}{\kappa_m+g_b(\kappa_2-\kappa_m)} \end{cases} \quad (A5)$$

Figs. A1(b) and (c) show qualitative and quantitative results of the designed metadevice locating at the middle of background. The calculated thermal conductivity of Eq. (A4) is endowed to the background. External temperature are added at three directions (shown by black arrows) for testing the feature of omnidirection. For comparison, we also carry out simulations of the pure matrix case, in which data slightly deviate from the reference. Larger volume fractions and aspect ratios of inclusions will make the contrast sharper. These results confirm the validity of our theoretical formulas in three-dimensional and multi-component systems.

References

[1] Y. Li, W. Li, T.C. Han, X. Zheng, J.X. Li, B.W. Li, S.H. Fan, C.W. Qiu, Transforming heat transfer with thermal metamaterials and devices, Nat. Rev. Mater. (2021), doi:10.1038/s41578-021-00283-2.

[2] J.P. Huang, Theoretical thermotics: Transformation thermotics and extended theories for thermal metamaterials, Springer, 2020.

[3] C.Z. Fan, Y. Gao, J.P. Huang, Shaped graded materials with an apparent negative thermal conductivity, Appl. Phys. Lett. 92 (2008) 251907.

[4] T.Y. Chen, C.-N. Weng, J.S. Chen, Cloak for curvilinearly anisotropic media in conduction, Appl. Phys. Lett. 93 (2008) 114103.

[5] S. Narayana, Y. Sato, Heat flux manipulation with engineered thermal materials, Phys. Rev. Lett. 108 (2012) 214303.

[6] G.Q. Xu, X. Zhou, J.Y. Zhang, Bilayer thermal harvesters for concentrating temperature distribution, Int. J. Heat Mass Trans. 142 (2019) 118434.

[7] X. He, L.Z. Wu, Thermal transparency with the concept of neutral inclusion, Phys. Rev. E 88 (2013) 033201.

[8] L.W. Zeng, R.X. Song, Experimental observation of heat transparency, Appl. Phys. Lett. 104 (2014) 201905.

[9] T.C. Han, X. Bai, J.T.L. Thong, B.W. Li, C.W. Qiu, Full control and manipulation of heat signatures: Cloaking, camouflage and thermal metamaterials, Adv. Mater. 26 (2014) 1731.

[10] R. Hu, S.L. Zhou, Y. Li, D.Y. Lei, X.B. Luo, C.W. Qiu, Illusion thermotics, Adv. Mater. 30 (2018) 1707237.

[11] T.C. Han, X. Bai, D.L. Gao, J.T.L. Thong, B.W. Li, C.W. Qiu, Experimental demonstration of a bilayer thermal cloak, Phys. Rev. Lett. 112 (2014) 054302.

[12] T.Z. Yang, X. Bai, D.L. Gao, L.Z. Wu, B.W. Li, J.T. Thong, C.W. Qiu, Invisible sensors: Simultaneous sensing and camouflaging in multiphysical fields, Adv. Mater. 27 (2015) 7752.

[13] L.J. Xu, C.R. Jiang, J. Shang, R.Z. Wang, J.P. Huang, Periodic composites: Quasi-uniform heat conduction, janus thermal illusion, and illusion thermal diodes, Eur. Phys. J. B 90 (2017) 221.

[14] J.X. Li, Y. Li, W.Y. Wang, L.Q. Li, C.W. Qiu, Effective medium theory for thermal scattering off rotating structures, Opt. Express 28 (2020) 25894.

[15] J. Wang, G. Dai, J. Huang, Thermal metamaterial: Fundamental, application, and outlook, iScience 23 (2020) 101637.

[16] X.Y. Shen, Y. Li, C.R. Jiang, J.P. Huang, Temperature trapping: Energy-free maintenance of constant temperatures as ambient temperature gradients change, Phys. Rev. Lett. 117 (2016) 055501.

[17] J. Wang, J. Shang, J.P. Huang, Negative energy consumption of thermostats at ambient temperature: Electricity generation with zero energy maintenance, Phys. Rev. Appl. 11 (2019) 024053.

[18] P.C. Cao, Y. Li, Y.G. Peng, C.-W. Qiu, X.F. Zhu, High-order exceptional points in diffusive systems: Robust APT symmetry against perturbation and phase oscillation at APT symmetry breaking, ES Energy Environ. 7 (2020) 48.

[19] L.J. Xu, J.P. Huang, Active thermal wave cloak, Chin. Phys. Lett. 37 (2020) 120501.

[20] E.M. Dede, P. Schmalenberg, T. Nomura, M. Ishigaki, Design of anisotropic thermal conductivity in multilayer printed circuit boards, IEEE T. Compon. Pack. Man. 5 (2015) 1763.

[21] H.S. Choe, R. Prabhakar, G. Wehmeyer, et al., Ion write microthermics: Programing thermal metamaterials at the microscale, Nano Lett. 19 (2019) 3830.

[22] J.P. Huang, K.W. Yu, Enhanced nonlinear optical responses of materials: Composite effects, Phys. Rep. 431 (2006) 87.

[23] J.F. Wang, J.K. Carson, M.F. North, D.J. Cleland, A new approach to modelling the effective thermal conductivity of heterogeneous materials, Int. J Heat Mass Trans. 49 (2006) 3075.

[24] J.C.M.-G. XII, Colours in metal glasses and in metallic films, VII. colours in metal glasses, in metallic films, and in metallic solutions, Philos. Trans. R. Soc. London Ser. A 203 (1904) 385. 205 (1906) 237

[25] G. Bruggeman, Calculation of various physics constants in heterogeneous substances i. dielectricity constants and conductivity of mixed bodies from isotropic substances, Ann. Phys. (Leipzig) 24 (1935) 636.

[26] K.B. Kiradjieva, S.A. Halvorsenb, R.A.V. Gordera, S.D. Howisona, Maxwell-type models for the effective thermal conductivity of a porous material with radiative transfer in the voids, Int. J. Therm. Sci. 145 (2019) 106009.

[27] R.Z. Wang, J. Shang, J.P. Huang, Design and realization of thermal camouflage with many-particle systems, Int. J. Therm. Sci. 131 (2018) 14.

[28] J. Shang, C.R. Jiang, L.J. Xu, J.P. Huang, Many-particle thermal invisibility and diode from effective media, J. Heat Transfer 140 (2018) 092004.

[29] S. Yang, L.J. Xu, R.Z. Wang, J.P. Huang, Full control of heat transfer in single–particle structural materials, Appl. Phys. Lett. 111 (2017) 121908.

[30] L.J. Xu, S. Yang, J.P. Huang, Effectively infinite thermal conductivity and zero-index thermal cloak, Phys. Rev. Appl. 11 (2019) 034056.

[31] F. Sun, Y.C. Liu, Y.B. Yang, Z.H. Chen, S.L. He, Thermal surface transformation and its applications to heat flux manipulations, Opt. Express 27 (2019) 33758.

[32] D. Torrent, O. Poncelet, J.C. Batsale, Nonreciprocal thermal material by spatiotemporal modulation, Phys. Rev. Lett. 120 (2018) 125501.

[33] M. Camacho, B. Edwards, N. Engheta, Achieving asymmetry and trapping in diffusion with spatiotemporal metamaterials, Nat. Commun. 11 (2020) 3733.

[34] J. Wang, G.L. Dai, F.B. Yang, J.P. Huang, Designing bistability or multistability in macroscopic diffusive systems, Phys. Rev. E 101 (2020) 1804019.

[35] S.Y. Huang, J.W. Zhang, M. Wang, W. Lan, R. Hu, X.B. Luo, Macroscale thermal diode-like black box with high transient rectification ratio, ES Energy Environ 6 (2019) 51.

[36] T.C. Han, P. Yang, Y. Li, D.Y. Lei, B.W. Li, K. Hippalgaonkar, C.W. Qiu, Full-parameter omnidirectional thermal metadevices of anisotropic geometry, Adv. Mater. 30 (2018) 1804019.

[37] X.W. Zhang, X. He, L.Z. Wu, Ellipsoidal bifunctional thermal-electric transparent device, Comp. Struc. 234 (2020) 111717.

[38] P. Sheng, Theory for the dielectric function of granular composite media, Phys. Rev. Lett. 45 (1980) 60.

[39] A.V. Goncharenko, Generalizations of the bruggeman equation and a concept of shape-distributed particle composites, Phys. Rev. E 68 (2003) 041108.

[40] H.L. Duan, B.L. Karihaloo, J. Wang, X. Yi, Effective conductivities of heterogeneous media containing multiple inclusions with various spatial distributions, Phys. Rev. B 73 (2006) 174203.

[41] O. Ouchetto, C.-W. Qiu, S. Zouhdi, L.W. Li, A. Razek, Homogenization of 3-d periodic bianisotropic metamaterials, IEEE Trans. Microwave Theory Tech. 54 (2006) 3893.

[42] Y. Gao, J.P. Huang, Y.M. Liu, L. Gao, K.W. Yu, X. Zhang, Optical negative refraction in ferrofluids with magneto-controllability, Phys. Rev. Lett. 104 (2010) 034501.

[43] H.L. Fu, L. Gao, Theory for anisotropic thermal conductivity of magnetic nanofluids, Phys. Lett. A 375 (2011) 3588.

[44] http://www.comsol.com/.

[45] A. Baule, R. Mari, L. Bo, L. Portal, H.A. Makse, Mean-field theory of random close packings of axisymmetric particles, Nat. Commun. 4 (2013) 2194.

[46] K. Chen, G. Ding, G. Hu, Z. Jin, J. Zhao, Y. Feng, T. Jiang, A. Alu, C.W. Qiu, Directional janus metasurface, Adv. Mater. 32 (2019) 1906352.

[47] V.A. Markel, Introduction to the maxwell garnett approximation: Tutorial, J. Opt. Soc. Am. A 33 (2016) 2237.

[48] D.K. Ma, A. Arora, S. Deng, G. Xie, J. Shiomi, N. Yang, Quantifying phonon particle and wave transport in silicon nanophononic metamaterial with cross junction, Mater. Today Phys. 8 (2019) 56.

[49] X. Zheng, B.W. Li, Effect of interfacial thermal resistance in a thermal cloak, Phys. Rev. Appl. 13 (2020) 024071.

[50] G.Q. Gu, K.W. Yu, P.M. Hui, First-principles approach to conductivity of a nonlinear composite, Phys. Rev. B 58 (1998) 3057.

[51] G.L. Dai, J.P. Huang, Nonlinear thermal conductivity of periodic composites, Int. J. Heat Mass Transfer 147 (2020) 118917.